



Angle-dependent high-order harmonic generation in a topological phase transition of monolayer black phosphorus

Rui Qin ¹ and Zi-Yu Chen ^{2,*}

¹National Key Laboratory of Shock Wave and Detonation Physics, Institute of Fluid Physics, China Academy of Engineering Physics, Mianyang 621999, China

²Key Laboratory of High Energy Density Physics and Technology (MoE), College of Physics, Sichuan University, Chengdu 610064, China



(Received 21 January 2024; accepted 7 March 2024; published 1 April 2024)

Identifying all-optical high-order harmonic observables as reliable signatures to probe the topology of matter has triggered intense interest. Recently, extensive *ab initio* simulations challenged the previously explored approaches and proposed a new potential feature, i.e., angular dependence of harmonic yield, as a possible fingerprint of material topology [O. Neufeld *et al.*, *Phys. Rev. X* **13**, 031011 (2023)]. However, nontopological contributions from the band structure, spin-orbit coupling (SOC), and Berry curvature have not been ruled out. Here, we clarify this point by studying the elaborately chosen sample system of monolayer black phosphorus, which exhibits similar band structures and are free from SOC as well as Berry curvature effects for both the trivial and topological phases induced by strain. We find the previously proposed angle-dependent harmonic difference to vanish, suggesting it to be an unreliable observable to probe material topology.

DOI: [10.1103/PhysRevA.109.043102](https://doi.org/10.1103/PhysRevA.109.043102)

I. INTRODUCTION

Nonperturbative high-order harmonic generation (HHG) in condensed matter systems has been extensively investigated over the past decade [1–3]. This extreme nonlinear optical phenomenon not only offers opportunities to achieve a new generation of solid-state compact coherent light sources and attosecond photonics in the extreme ultraviolet short-wavelength range, but also enables fascinating all-optical exploration of electronic structures and ultrafast dynamics in interested materials in the strong-field and nonequilibrium regime. Representative demonstrations include the observation of sub-laser-cycle Bloch oscillation dynamics [4,5], retrieval of electronic band structures [6–8], picometer-scale real-space imaging of valence electron structures [9], and reconstruction of Berry curvatures in crystalline solids [10].

In addition to conventional semiconductors and insulators, HHG spectroscopy in solids has been extended to study other novel and complex materials, such as Dirac semimetals [11–17], Weyl semimetals [18], Mott insulators [19,20], topological insulators [21–30], topological semiconductors [31], and topological semimetals [32,33]. Among these material systems, topological materials have attracted considerable interest because of their intriguing physics linked to the mathematical concept of topology and also their potential applications associated with the robustness against nonmagnetic perturbations. Various works, taking both theoretical and experimental approaches, have been carried out, attempting to find marks of topological effects on the HHG characteristics. However, it is very challenging to extract exact information distinguishing topologically trivial and nontrivial

phases of matter. Whether the reported observables are truly HHG signatures for probing topology remains a controversial topic. One of the major difficulties is that most theoretical studies employ simplified models neglecting various physical effects and the interpretations for experimental measurements largely rely on the approximated model results.

In comparison to a simplified model analysis, *ab initio* simulations allow many properties of real materials to be considered, such as the complete electronic band structures rather than just a few active bands, electron-electron interactions, and electron-ion interactions. Recently, Neufeld *et al.* [34] report a thorough *ab initio* time-dependent density functional theory (TDDFT) simulation study of HHG from exemplary topological insulators to clarify the link between previously studied HHG signatures and material topology. As they find, the previously proposed topological observables, including HHG helicity, anomalous HHG ellipticity, HHG elliptical dichroism, and temporal delays in HHG emission, can all be excluded from reliable and general fingerprints identifying topological characters of materials. Nevertheless, they discover one potentially promising feature of HHG spectroscopy that might drop a hint on topological signatures, which is the angular dependence of the parallel HHG yield driven by linearly polarized lasers varying strikingly between topologically trivial and nontrivial phases of two-dimensional bismuthane (BiH). BiH monolayer is a topologically trivial semimetal in the absence of spin-orbit coupling (SOC), while it is turned into a topological insulator with SOC considered. Yet, the authors also point out that their studies cannot lead to a decisive conclusion that the angle-dependent HHG yield can be viewed as a fingerprint of material topology. This is because some other possible contributions, independent of topology, cannot be excluded from their studied systems. These major issues include the band structure, SOC, and

*ziyuch@scu.edu.cn

Berry curvature, which can all significantly affect the electron dynamics and hence HHG processes. In their simulated material systems, however, the topologically trivial and nontrivial BiH have markedly different band structures. In addition, the topologically trivial BiH is obtained without SOC, in contrast to the topologically nontrivial phase with SOC.

In this paper, we perform *ab initio* TDDFT simulations to elucidate the question of angle-dependent parallel HHG yield as a possible signature of topology. To rule out the nontopology contributions to the HHG difference between trivial and topological phases from different band structures, SOC, or Berry curvature, we meticulously choose monolayer black phosphorus (BP) as the sample system, in which the topological phase transition is induced by a strain effect rather than SOC. The SOC effect is absent for both phases. The Berry curvature also remains zero during the transition due to the symmetry. The electronic state is altered under strain to form band inversion accompanied by the \mathbb{Z}_2 number changing from 0 to 1, while the band structures before and after the phase transition are very similar. Under such circumstances, our simulation results show that the previously reported evident deviation of angular dependence for parallel HHG yield between the two phases disappears, suggesting that the feature of angle-dependent parallel HHG is also an unreliable signature of a topological phase.

II. MATERIALS AND METHODS

Monolayer BP is studied by using a periodic supercell model. The lattice constant along the direction perpendicular to the BP layer (z direction) is taken to be 15 Å to eliminate the interactions between adjacent monolayer BP images. The atomic structure of monolayer BP is optimized within the density functional theory framework using the QUANTUM ESPRESSO package [35,36]. The generalized gradient approximation (GGA) of the Perdew-Burke-Ernzerhof (PBE) form [37] is employed for the exchange-correlation functional, and the van der Waals interaction correction is considered by the Grimme-D2 semiempirical correction [38]. A plane-wave cutoff energy of 48 Ry, the norm-conserving PSEUDODOJO pseudopotential [39], and an $8 \times 10 \times 1$ Monkhorst-Pack k -point mesh [40] for Brillouin zone sampling are used in the calculations. The atomic positions are relaxed until all components of the force on each atom is less than 0.001 eV/Å.

The time evolution of the wave functions and the time-dependent total electronic current are studied by propagating the time-dependent Kohn-Sham equations in real time and real space within the framework of TDDFT with the adiabatic GGA of the PBE form using the OCTOPUS code [41,42] which uses the real-space grid representation. For the study of the time evolution properties, the lattice constant along the direction perpendicular to the layer is taken to be 30 bohrs, which includes 3 bohrs of absorbing regions on each side of the layer to avoid a reflection error in the spectral region of interest. The grid spacing of the real-space box is 0.46 bohrs, and the time step for temporal propagation is 6.05 attosecond (as). A $36 \times 48 \times 1$ Monkhorst-Pack k -point mesh for Brillouin zone sampling and the PSEUDODOJO pseudopotential are used in the calculations.

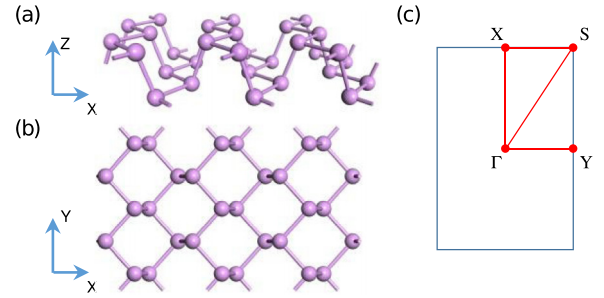


FIG. 1. Crystal structures and Brillouin zone of monolayer black phosphorus (BP). (a) Side view and (b) top view of the crystal structure of monolayer BP, and (c) Brillouin zone and high-symmetry k points of monolayer BP.

The driving laser field is described in the velocity gauge. The laser wavelength is 1600 nm. The laser field is linearly polarized in the plane of the two-dimensional (2D) structure. The laser pulse has a sine-square envelope $f(t) = \sin^2(\pi t/2\tau)$ with $\tau = 20$ fs and the carrier-envelope phase is set to be zero. The peak laser intensity is 2×10^{11} W/cm².

The HHG spectrum is calculated from the time-dependent electronic current $\mathbf{j}(\mathbf{r}, t)$ as

$$\text{HHG}(\omega) = \left| \mathcal{FT} \left(\frac{\partial}{\partial t} \int \mathbf{j}(\mathbf{r}, t) d^3\mathbf{r} \right) \right|^2, \quad (1)$$

where \mathcal{FT} denotes the Fourier transform.

III. RESULTS AND DISCUSSION

A. Crystal and electronic structures

The crystal structure of monolayer BP is shown in Figs. 1(a) and 1(b). It is a puckered structure containing two layers of phosphorus atoms, and each phosphorus atom is covalently bonded to three adjacent phosphorus atoms. The coordinate system used in this work is denoted in Fig. 1, with Fig. 1(c) displaying the Brillouin zone and high-symmetry k points. For monolayer BP without strain, the optimized in-plane lattice constants along the x (armchair) and y (zigzag) directions are $a = 4.57$ Å and $b = 3.31$ Å, respectively, which are in good agreement with previous theoretical results [43]. The separation between the two layers of phosphorus atoms is 2.11 Å. A vertical tensile strain is then gradually applied to trigger a topological transition in monolayer BP. In our calculations, strain ϵ is defined as $\epsilon = (c - c_0)/c_0$, where c and c_0 are the layer separation with and without strain, respectively. For each strain, the in-plane lattice constants and atom positions are fully relaxed.

We first investigate the electronic structures of monolayer BP under strain. As previous theoretical results [43,44], a highly asymmetric band dispersion around the Γ point is seen. Both the valence and conduction bands are relatively flat along the Γ - X direction, while they are significantly dispersive along the Γ - Y direction. The direct band gap at the Γ point for monolayer BP without strain is calculated to be 0.87 eV, which is lower than the experimental result (1.45 eV) [45] due to the well-known underestimated band-gap problem of the GGA exchange-correlation functional. Yet this only has little effect on the HHG [44]. When tensile strain increases,

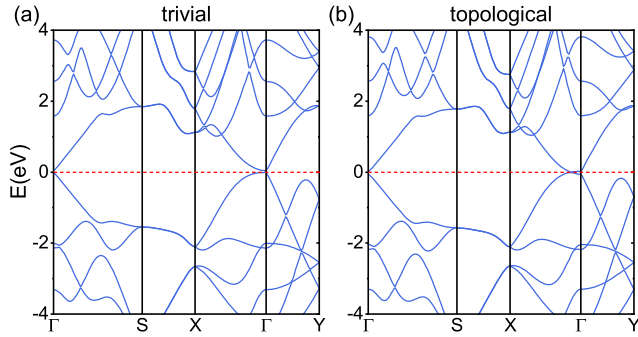


FIG. 2. Band structures of the (a) trivial and (b) topological phases of monolayer BP at strains of 7.8% and 8.8%, respectively.

the direct band gap decreases, and the band dispersion remains highly asymmetric around the Γ point [Fig. 2(a)]. The valence band maximum (VBM) and conduction band minimum (CBM) will finally touch at the Γ point, and the band gap closes at a critical tensile strain of 8.3%, which agrees with previous theoretical calculations [46]. For strains larger than the critical strain, the lowest conduction band and highest valence band begin to overlap and intersect at the Γ -X line near the Γ point [Fig. 2(b)]. Thus monolayer BP undergoes a semiconductor-metal transition when vertical tensile strain is applied.

In addition to the band gap closing, the topological properties of the electronic structures of monolayer BP also change under strain. Due to the symmetry of the crystal structure, the bands of monolayer BP have well-defined parities. It has been shown that the VBM and CBM have opposite parities [47,48]. After critical strain, the lowest conduction band and highest valence band begin to cross. Thus the band order and parities are inverted at the Γ point, and the so-called band inversion occurs. Since the parities of the bands far from the Γ point are unchanged and only inverted when approaching the Γ point, the top valence band and bottom conduction band should remain contacted to ensure a continuous symmetry evolution.

Previously, bilayer BP under strain [49] and few-layer BP applied with electric field [47] are found to undergo a normal-to-topological phase transition. However, whether monolayer BP can be switched into a topological phase by strain is unknown. To confirm our studied monolayer BP under strain is truly a topological phase, we further calculate the topological invariant number \mathbb{Z}_2 by using Soluyanov's method [50] implemented in the WANNIERTOOLS package [51]. The calculated \mathbb{Z}_2 numbers are found to be 0 and 1 before and after the critical strains, respectively. Therefore, monolayer BP indeed undergoes a topological transition along with the band gap closing under the strain. We note the band structures change only slightly during the transition, while the topological properties change significantly. In addition, the topological transition in this work is totally unrelated to the spin-orbital interaction. Moreover, the topological and trivial phases both exhibit zero Berry curvatures, since the monolayer BP samples keep inversion symmetry before and after the topological transition. Therefore, the topological phase transition by means of strain in monolayer BP can serve as a clean and desirable platform to clarify the topological effect on the HHG response.

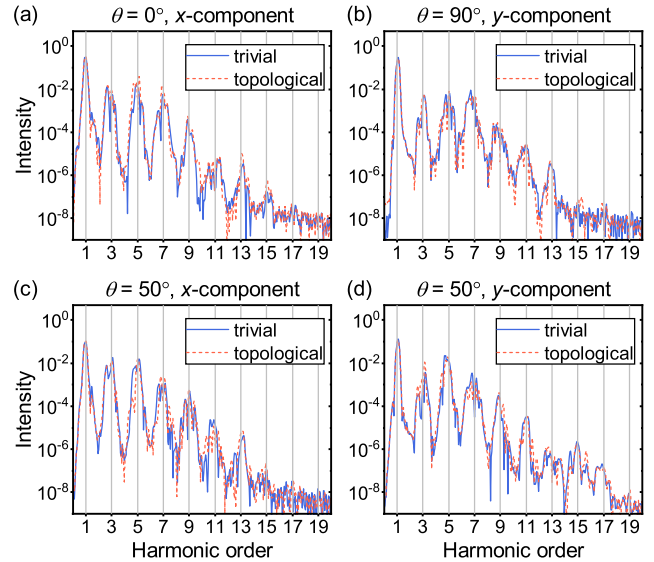


FIG. 3. HHG spectra from both trivial and topological phases of monolayer BP for different harmonic components and laser polarization angle θ . (a) x component with $\theta = 0^\circ$; (b) y component with $\theta = 90^\circ$; (c) x and (d) y components with $\theta = 50^\circ$. θ is defined as the angle between the x axis and the driving laser polarization direction.

B. HHG

We then investigate the high-order harmonic spectral properties in the topological transition. We focus on the angular dependence of the HHG yield driven by linearly polarized lasers, which is suggested as a likely candidate of topological signature by the previous work of Neufeld *et al.* [34]. A linearly polarized laser is applied to monolayer BP at strain values of 7.8% and 8.8%, which characterize trivial and topological phases, respectively.

Before addressing the angular dependence of HHG between the trivial and topological phases, we take a look at the general properties of high-order harmonic spectra of monolayer BP driven by a linearly polarized laser with various polarization angles θ , which is defined as the angle between the x axis and the driving laser polarization direction. The results are shown in Fig. 3. When the laser is polarized along the x ($\theta = 0^\circ$) and y ($\theta = 90^\circ$) directions, there are no transverse harmonics for the electric current and thus high-order harmonics due to the high symmetry of the system Hamiltonians. For $\theta = 0^\circ$, the high-order harmonic spectra of both trivial and topological phases are nearly the same with a cutoff order of 15, and only the amplitude of the high-order harmonics of the topological phase is slightly larger than that of the trivial phase [Fig. 3(a)]. For $\theta = 90^\circ$, the high-order harmonic spectra are quite different from those of the $\theta = 0^\circ$ case due to the anisotropy of monolayer BP. However, the difference between high-order harmonic spectra of trivial and topological phases is also quite small, except the high-order harmonic spectrum of the topological phase being cleaner than that of the trivial phase for high-order harmonic orders [Fig. 3(b)]. When the laser is polarized in asymmetrical directions, the transverse component of HHG is observed due to the broken symmetry. As shown in Figs. 3(c) and 3(d), the x and y components of HHG are out of proportion and have large differences in

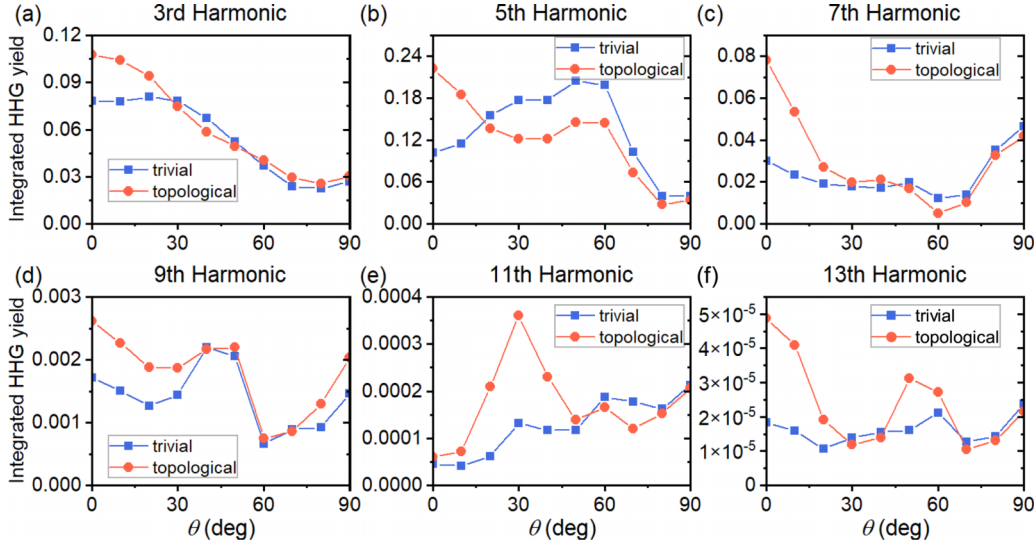


FIG. 4. HHG yield of components parallel to the laser polarization direction vs laser polarization angle θ for different harmonic orders from both trivial and topological phases of monolayer BP driven by a linearly polarized laser.

spectral shape and cutoff order. Nevertheless, there is still little difference between the high-order harmonic spectra of trivial and topological phases.

Figure 4 shows the HHG yield of the harmonic component parallel to the laser polarization direction as a function of angle θ for various harmonic orders from the third order to the 13th order. The HHG yield shows a mirror symmetry around $\theta = 90^\circ$ due to the crystal symmetry. Thus we only plot the HHG yield for θ between 0° and 90° . For each harmonic order, an important and striking feature can be clearly observed that the variation trends of HHG yield versus laser polarization direction are generally very similar between the topological and trivial phases. Although there are very few exceptions, e.g., $\theta \leq 20^\circ$ for the fifth harmonic, they do not show a clear and regular pattern across all harmonics. This similar variation is in sharp contrast to the result obtained

by Neufeld *et al.* [34], which display marked differences of angular dependence between the two phases. Note that the sample systems studied in Ref. [34] exhibit very different band structures and SOC between the two phases, which are generically independent of the topology. However, when these nontopological contributions are all eliminated in our sample systems, the difference in angular dependence between the two phases disappears. This result strongly suggests that the previously proposed deviation of angular dependence for the parallel HHG yield between the two phases is most probably attributed to the aforementioned nontopological effects and should not be viewed as a robust and reliable topological signature in HHG as well.

As for the transverse harmonic components, the angular dependence of HHG yield between the two phases also displays very similar features for all harmonic orders from the

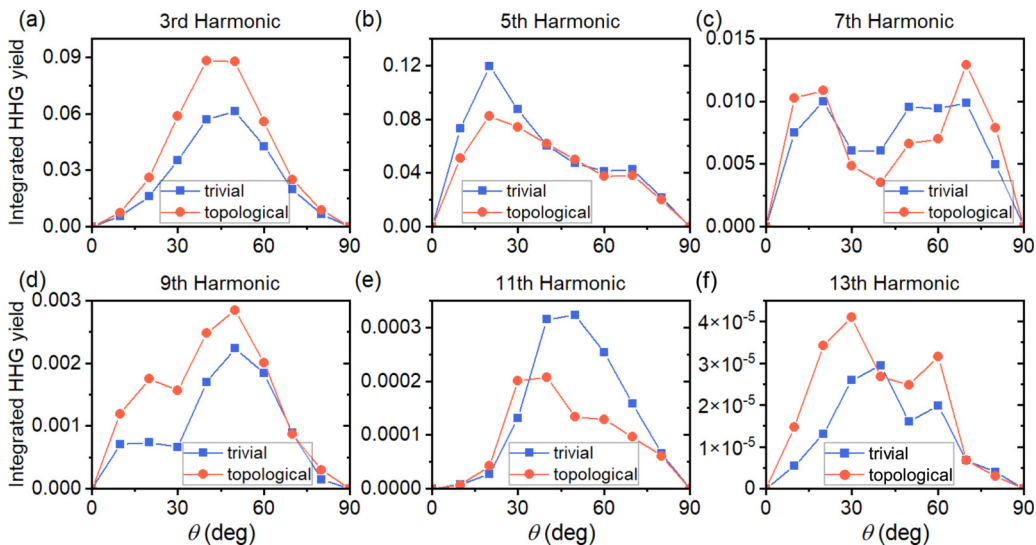


FIG. 5. HHG yield of components transverse to the laser polarization direction vs laser polarization angle θ for different harmonic orders from both trivial and topological phases of monolayer BP driven by the linearly polarized laser.

third to the 13th, as can be seen in Fig. 5. The differences are even smaller than that of the parallel harmonic components. This result is in agreement with that presented by Neufeld *et al.* [34], which can be explained by the transverse component being more sensitive to the crystal symmetries rather than the topological nature or band structures.

IV. CONCLUSIONS

In conclusion, we have performed an *ab initio* study of HHG from topological and trivial phases of monolayer BP under strain driven by linearly polarized lasers along various crystal orientations. The angular dependence of the HHG yield for both parallel and transverse components shows very similar variation behaviors between the two phases. As our chosen sample system exhibits similar band structures, SOC,

and Berry curvatures for both phases, the result may rule out the previously proposed observable of angular dependence deviation as a high-order harmonic signature of topology, which was based on the *ab initio* calculations of a 2D BiH system exhibiting very different band structures and SOC for topological and trivial phases. Our results thus clarify the origin of angle-dependent features in linearly polarized laser-driven HHG and advance the understanding of high-order harmonic spectroscopy as possible tools to probe the topology of matter.

ACKNOWLEDGMENT

This work was supported in part by the National Natural Science Foundation of China (Grants No. 12274382 and No. 12175157).

-
- [1] S. Ghimire, A. D. DiChiara, E. Sistrunk, P. Agostini, L. F. DiMauro, and D. A. Reis, Observation of high-order harmonic generation in a bulk crystal, *Nat. Phys.* **7**, 138 (2011).
- [2] S. Ghimire and D. A. Reis, High-harmonic generation from solids, *Nat. Phys.* **15**, 10 (2019).
- [3] E. Goulielmakis and T. Brabec, High harmonic generation in condensed matter, *Nat. Photon.* **16**, 411 (2022).
- [4] O. Schubert, M. Hohenleutner, F. Langer, B. Urbanek, C. Lange, U. Huttner, D. Golde, T. Meier, M. Kira, S. W. Koch, and R. Huber, Sub-cycle control of terahertz high-harmonic generation by dynamical Bloch oscillations, *Nat. Photon.* **8**, 119 (2014).
- [5] T. T. Luu, M. Garg, S. Y. Kruchinin, A. Moulet, M. T. Hassan, and E. Goulielmakis, Extreme ultraviolet high-harmonic spectroscopy of solids, *Nature (London)* **521**, 498 (2015).
- [6] G. Vampa, T. J. Hammond, N. Thiré, B. E. Schmidt, F. Légaré, C. R. McDonald, T. Brabec, D. D. Klug, and P. B. Corkum, All-optical reconstruction of crystal band structure, *Phys. Rev. Lett.* **115**, 193603 (2015).
- [7] A. A. Lanin, E. A. Stepanov, A. B. Fedotov, and A. M. Zheltikov, Mapping the electron band structure by intraband high-harmonic generation in solids, *Optica* **4**, 516 (2017).
- [8] L. Li, P. Lan, L. He, W. Cao, Q. Zhang, and P. Lu, Determination of electron band structure using temporal interferometry, *Phys. Rev. Lett.* **124**, 157403 (2020).
- [9] H. Lakhota, H. Y. Kim, M. Zhan, S. Hu, S. Meng, and E. Goulielmakis, Laser picoscopy of valence electrons in solids, *Nature (London)* **583**, 55 (2020).
- [10] T. T. Luu and H. J. Wörner, Measurement of the Berry curvature of solids using high-harmonic spectroscopy, *Nat. Commun.* **9**, 916 (2018).
- [11] N. Yoshikawa, T. Tamaya, and K. Tanaka, High-harmonic generation in graphene enhanced by elliptically polarized light excitation, *Science* **356**, 736 (2017).
- [12] M. Taucer, T. J. Hammond, P. B. Corkum, G. Vampa, C. Couture, N. Thiré, B. E. Schmidt, F. Légaré, H. Selvi, N. Unsurree, B. Hamilton, T. J. Echtermeyer, and M. A. Denecke, Nonperturbative harmonic generation in graphene from intense midinfrared pulsed light, *Phys. Rev. B* **96**, 195420 (2017).
- [13] M. Baudisch, A. Marini, J. D. Cox, T. Zhu, F. Silva, S. Teichmann, M. Massicotte, F. Koppens, L. S. Levitov, F. J. García de Abajo, and B. Jens, Ultrafast nonlinear optical response of Dirac fermions in graphene, *Nat. Commun.* **9**, 1018 (2018).
- [14] R. Qin and Z.-Y. Chen, Strain-controlled high harmonic generation with Dirac fermions in silicene, *Nanoscale* **10**, 22593 (2018).
- [15] Z.-Y. Chen and R. Qin, Circularly polarized extreme ultraviolet high harmonic generation in graphene, *Opt. Express* **27**, 3761 (2019).
- [16] Z.-Y. Chen and R. Qin, High harmonic generation in graphene-boron nitride heterostructures, *J. Mater. Chem. C* **8**, 12085 (2020).
- [17] S. Kovalev, R. M. A. Dantas, S. Germanskiy, J.-C. Deinert, B. Green, I. Ilyakov, N. Awari, M. Chen, M. Bawatna, J. Ling, F. Xiu, P. H. M. van Loosdrecht, P. Surówka, T. Oka, and Z. Wang, Non-perturbative terahertz high-harmonic generation in the three-dimensional Dirac semimetal Cd₃As₂, *Nat. Commun.* **11**, 2451 (2020).
- [18] Y.-Y. Lv, J. Xu, S. Han, C. Zhang, Y. Han, J. Zhou, S.-H. Yao, X.-P. Liu, M.-H. Lu, H. Weng, Z. Xie, Y. B. Chen, J. Hu, Y.-F. Chen, and S. Zhu, High-harmonic generation in Weyl semimetal β -WP₂ crystals, *Nat. Commun.* **12**, 6437 (2021).
- [19] Y. Murakami, M. Eckstein, and P. Werner, High-harmonic generation in Mott insulators, *Phys. Rev. Lett.* **121**, 057405 (2018).
- [20] C. Orthodoxou, A. Zaïr, and G. H. Booth, High harmonic generation in two-dimensional Mott insulators, *npj Quantum Mater.* **6**, 76 (2021).
- [21] D. Bauer and K. K. Hansen, High-harmonic generation in solids with and without topological edge states, *Phys. Rev. Lett.* **120**, 177401 (2018).
- [22] R. E. F. Silva, A. Jiménez-Galán, B. Amorim, O. Smirnova, and M. Ivanov, Topological strong-field physics on sub-laser-cycle timescale, *Nat. Photon.* **13**, 849 (2019).
- [23] A. Chacón, D. Kim, W. Zhu, S. P. Kelly, A. Dauphin, E. Pisanty, A. S. Maxwell, A. Picón, M. F. Ciappina, D. E. Kim, C. Ticknor, A. Saxena, and M. Lewenstein, Circular dichroism in higher-order harmonic generation: Heralding topological

- phases and transitions in Chern insulators, *Phys. Rev. B* **102**, 134115 (2020).
- [24] Y. Bai, F. Fei, S. Wang, N. Li, X. Li, F. Song, R. Li, Z. Xu, and P. Liu, High-harmonic generation from topological surface states, *Nat. Phys.* **17**, 311 (2021).
- [25] D. Baykusheva, A. Chacón, J. Lu, T. P. Bailey, J. A. Sobota, H. Soifer, P. S. Kirchmann, C. Rotundu, C. Uher, T. F. Heinz, D. A. Reis, and S. Ghimire, All-optical probe of three-dimensional topological insulators based on high-harmonic generation by circularly polarized laser fields, *Nano Lett.* **21**, 8970 (2021).
- [26] C. P. Schmid, L. Weigl, P. Grössing, V. Junk, C. Gorini, S. Schlauderer, S. Ito, M. Meierhofer, N. Hofmann, D. Afanasiev, J. Crewse, K. A. Kokh, O. E. Tereshchenko, J. Güdde, F. Evers, J. Wilhelm, K. Richter, U. Höfer, and R. Huber, Tunable non-integer high-harmonic generation in a topological insulator, *Nature (London)* **593**, 385 (2021).
- [27] D. Baykusheva, A. Chacón, D. Kim, D. E. Kim, D. A. Reis, and S. Ghimire, Strong-field physics in three-dimensional topological insulators, *Phys. Rev. A* **103**, 023101 (2021).
- [28] Y. Bai, N. Li, R. Li, and P. Liu, Ultrafast dynamics of helical Dirac fermions in the topological insulators, *Adv. Phys.: X* **7**, 2013134 (2022).
- [29] C. Heide, Y. Kobayashi, D. R. Baykusheva, D. Jain, J. A. Sobota, M. Hashimoto, P. S. Kirchmann, S. Oh, T. F. Heinz, D. A. Reis, and S. Ghimire, Probing topological phase transitions using high-harmonic generation, *Nat. Photon.* **16**, 620 (2022).
- [30] C. Qian, C. Yu, S. Jiang, T. Zhang, J. Gao, S. Shi, H. Pi, H. Weng, and R. Lu, Role of shift vector in high-harmonic generation from noncentrosymmetric topological insulators under strong laser fields, *Phys. Rev. X* **12**, 021030 (2022).
- [31] J. Shi, H. Xu, C. Heide, C. HuangFu, C. Xia, F. de Quesada, H. Shen, T. Zhang, L. Yu, A. Johnson, F. Liu, E. Shi, L. Jiao, T. Heinz, S. Ghimire, J. Li, J. Kong, Y. Guo, and A. M. Lindenberg, Giant room-temperature nonlinearities in a monolayer Janus topological semiconductor, *Nat. Commun.* **14**, 4953 (2023).
- [32] C. H. Lee, H. H. Yap, T. Tai, G. Xu, X. Zhang, and J. Gong, Enhanced higher harmonic generation from nodal topology, *Phys. Rev. B* **102**, 035138 (2020).
- [33] N. Tancogne-Dejean, F. G. Eich, and A. Rubio, Effect of spin-orbit coupling on the high harmonics from the topological Dirac semimetal Na_3Bi , *npj Comput. Mater.* **8**, 145 (2022).
- [34] O. Neufeld, N. Tancogne-Dejean, H. Hübener, U. De Giovannini, and A. Rubio, Are there universal signatures of popological phases in high-harmonic generation? Probably not, *Phys. Rev. X* **13**, 031011 (2023).
- [35] P. Giannozzi, S. Baroni, N. Bonini, M. Calandra, R. Car, C. Cavazzoni, D. Ceresoli, G. L. Chiarotti, M. Cococcioni, I. Dabo, A. D. Corso, S. d. Gironcoli, S. Fabris, G. Fratesi, R. Gebauer, U. Gerstmann, C. Gougoussis, A. Kokalj, M. Lazzeri, L. Martin-Samos *et al.*, QUANTUMESPRESSO: A modular and open-source software project for quantum simulations of materials, *J. Phys.: Condens. Matter* **21**, 395502 (2009).
- [36] P. Giannozzi, O. Andreussi, T. Brumme, O. Bunau, M. B. Nardelli, M. Calandra, R. Car, C. Cavazzoni, D. Ceresoli, M. Cococcioni, N. Colonna, I. Carnimeo, A. D. Corso, S. de Gironcoli, P. Delugas, R. A. DiStasio, A. Ferretti, A. Floris, G. Fratesi, G. Fugallo *et al.*, Advanced capabilities for materials modelling with QUANTUM ESPRESSO, *J. Phys.: Condens. Matter* **29**, 465901 (2017).
- [37] J. P. Perdew, K. Burke, and M. Ernzerhof, Generalized gradient approximation made simple, *Phys. Rev. Lett.* **77**, 3865 (1996).
- [38] S. Grimme, Semiempirical GGA-type density functional constructed with a long-range dispersion correction, *J. Comput. Chem.* **27**, 1787 (2006).
- [39] M. van Setten, M. Giantomassi, E. Bousquet, M. Verstraete, D. Hamann, X. Gonze, and G.-M. Rignanese, The PSEUDO-DOJO: Training and grading a 85 element optimized norm-conserving pseudopotential table, *Comput. Phys. Commun.* **226**, 39 (2018).
- [40] H. J. Monkhorst and J. D. Pack, Special points for Brillouin-zone integrations, *Phys. Rev. B* **13**, 5188 (1976).
- [41] X. Andrade, D. Strubbe, U. De Giovannini, A. H. Larsen, M. J. T. Oliveira, J. Alberdi-Rodriguez, A. Varas, I. Theophilou, N. Helbig, M. J. Verstraete, L. Stella, F. Nogueira, A. Aspuru-Guzik, A. Castro, M. A. L. Marques, and A. Rubio, Real-space grids and the OCTOPUS code as tools for the development of new simulation approaches for electronic systems, *Phys. Chem. Chem. Phys.* **17**, 31371 (2015).
- [42] N. Tancogne-Dejean, M. J. T. Oliveira, X. Andrade, H. Appel, C. H. Borca, G. Le Breton, F. Buchholz, A. Castro, S. Corni, A. A. Correa, U. De Giovannini, A. Delgado, F. G. Eich, J. Flick, G. Gil, A. Gomez, N. Helbig, H. Hübener, R. Jöstädt, J. Jorner-Somoza *et al.*, OCTOPUS, a computational framework for exploring light-driven phenomena and quantum dynamics in extended and finite systems, *J. Chem. Phys.* **152**, 124119 (2020).
- [43] J. Qiao, X. Kong, Z.-X. Hu, F. Yang, and W. Ji, High-mobility transport anisotropy and linear dichroism in few-layer black phosphorus, *Nat. Commun.* **5**, 4475 (2014).
- [44] Z.-Y. Chen and R. Qin, Strong-field nonlinear optical properties of monolayer black phosphorus, *Nanoscale* **11**, 16377 (2019).
- [45] H. Liu, A. T. Neal, Z. Zhu, Z. Luo, X. Xu, D. Tománek, and P. D. Ye, Phosphorene: An unexplored 2D semiconductor with a high hole mobility, *ACS Nano* **8**, 4033 (2014).
- [46] G. Q. Huang and Z. W. Xing, Band-gap tunability and dynamical instability in strained monolayer and bilayer phosphorenes, *J. Phys.: Condens. Matter* **27**, 175006 (2015).
- [47] Q. Liu, X. Zhang, L. B. Abdalla, A. Fazzio, and A. Zunger, Switching a normal insulator into a topological insulator via electric field with application to phosphorene, *Nano Lett.* **15**, 1222 (2015).
- [48] R. Fei, V. Tran, and L. Yang, Topologically protected Dirac cones in compressed bulk black phosphorus, *Phys. Rev. B* **91**, 195319 (2015).
- [49] T. Zhang, J.-H. Lin, Y.-M. Yu, X.-R. Chen, and W.-M. Liu, Stacked bilayer phosphorene: strain-induced quantum spin Hall state and optical measurement, *Sci. Rep.* **5**, 13927 (2015).
- [50] A. A. Soluyanov and D. Vanderbilt, Wannier representation of \mathbb{Z}_2 topological insulators, *Phys. Rev. B* **83**, 035108 (2011).
- [51] Q. Wu, S. Zhang, H.-F. Song, M. Troyer, and A. A. Soluyanov, WANNIERTOOLS: An open-source software package for novel topological materials, *Comput. Phys. Commun.* **224**, 405 (2018).